A molecular explanation for anomalous diffusion in supramolecular polymer networks

*Jorge Ramirez,[1,2] Thomas J. Dursch,[1] Bradley D. Olsen[1]**

[1] Department of Chemical Engineering, Massachusetts Institute of Technology, Cambridge, MA 02139, USA

[2] Department of Chemical Engineering, Universidad Politécnica de Madrid, Madrid, Spain

KEYWORDS:

Supramolecular, associative polymer, diffusion, hopping, Brownian dynamics, network.

ABSTRACT

Recent experiments have revealed that a variety of associative polymers with different architecture (linear and branched) and different nature of the associating interaction (associative protein domains and metal-ligand bonds) exhibit unexplained superdiffusive behavior. Here, Brownian dynamics simulations of unentangled coarse-grained associating star-shaped polymers are used to establish a molecular picture of chain dynamics that explains this behavior. Polymers are conceptualized as particles with effective Rouse diffusivities that interact with a mean field background through attachments by stickers at the end of massless springs that represent the arms of the polymer. The simulations reveal three mechanisms of molecular diffusion at length scales

much larger than the radius of gyration: hindered diffusion, walking diffusion, and molecular hopping, all of which depend strongly on polymer concentration, arm length, and the association/dissociation rate constants. The molecular model establishes that superdiffusive scaling results primarily from molecular hopping, which only occurs when the kinetics of attachment are slower than the relaxation time of dangling strands. Scaling relationships can be used to identify the range of rate constants over which this behavior is expected. The formation of loops in the networks promotes this superdiffusive scaling by reducing the total number of arms that must detach in order for a hopping step to occur.

INTRODUCTION

Supramolecular networks are an exciting class of soft materials with significant impact in fields as diverse as enhanced oil recovery [1], synthetic extracellular matrices for tissue engineering [2], injectable biomaterials for minimally invasive surgery [3,4], sacrificial components in tough and fatigue resistant physical double networks [5] and self-healing soft materials for autonomous damage repair [6]. In contrast to their chemically cross-linked counterparts, supramolecular networks are formed by temporary physical [7,8,9,10,11,12] or chemical bonds [7,8,13] whose rates of association/dissociation govern junction dynamics, and consequently, the rheological response of the network [10,11,12,14,15,16,17]. As a result of the transient nature of the bonds, associative polymers can inherently dissipate part of the stress stored in the network strands, and the constituent molecules can diffuse within the networks on length scales greater than their radius of gyration [1,10,11,12,14,18,19,20,21,22 23,24]. This allows the network to dynamically rearrange and to respond to mild external stimuli. Therefore, a quantitative description of molecular motion is critical to overcoming

important challenges such as predicting the rate of degradation of implantable biomaterials [25], determining the time scale of self-healing in networks [26], understanding how cells dynamically remodel hydrogels [27], and calculating the rheological response of shear-thinning materials [3].

Theoretical efforts have addressed supramolecular-network dynamics on the macroscopic and molecular levels [14,15,16,17,20,21,22,23,24,28]; however, knowledge of diffusive dynamics, especially self-diffusion, of the network-forming constituents remains limited [10,11,12]. Diffusion measurements provide a complementary probe of molecular dynamics to rheology, and comparison of dynamic theories with diffusion data provides critical insight into the testing and development of dynamic models. In addition, diffusion itself is an important dynamic property in many polymeric systems.

Recent studies [10,11,12,28] have shown that self-diffusive polymer dynamics often contain unexpected physics; in particular, apparent superdiffusive scaling regimes (i.e., when the distance versus time dependence is stronger than Fickian diffusion) are observed on length scales much larger than the radius of gyration of the polymers that make up the gel. Using forced Rayleigh scattering (FRS), Tang et al. [10,11,12] observed such superdiffusive regimes in metal coordinate star-polymer gels and associative linear coiled-coil protein gels. These non-Fickian scaling regimes are not predicted by the sticky Rouse/reptation theories [21,22,23,24], indicating that the state-of-the-art understanding of associative polymer dynamics is incomplete.

To explain the observed superdiffusive scaling regimes, Tang, Wang, and Olsen [10,11,12] developed an empirical two-state model where a diffusing species is in dynamic equilibrium between a molecular state ("fast") and an associated ("slow") state, and molecules can exchange between both states by means of first order reactions. Despite its seeming simplicity, the model quantitatively captured the transition from superdiffusive scaling at intermediate length scales to Fickian diffusion at large scales. In this Fickian regime, the effective diffusivity is governed by

the fast-state diffusivity and corresponding fraction of time spent in the fast state, whereas in the apparent superdiffusive regime, rate of diffusion is governed by the transition rate between the fast and slow diffusing states.

While the two-state model proved quantitatively accurate in predicting the dynamics of the materials, it does not provide insight into the detailed mechanisms underlying these surprising observations. Recently, Tirrell and coworkers [28] demonstrated that diffusion of telechelic molecules (i.e., with only two associative groups and three molecular associative states) measured by fluorescence recovery after photobleaching (FRAP) can be accurately captured by a three-state model accounting for all molecular states (zero, one, and two stickers attached to the network). While the ability of Tirrell and coworkers [28] to reduce the telechelic system to three states is intuitive based on the limited number of molecular configurations, the systems studied by Tang et al. [10,11,12] have significantly more than two molecular configurations, making the efficacy of the two-state model surprising.

Here, it is hypothesized that the superdiffusive scaling results from molecular hopping, where a molecule detaches completely from the network and diffuses a distance much larger than its own size. The goal of this work is to systematically test this hypothesis using molecular simulations. Specifically, Brownian dynamics of unentangled coarse-grained associating star-shaped polymers (a direct analog to the system studied experimentally in Reference [10]) is employed to capture the essential physics of self-diffusion in supramolecular networks. The model is validated through comparison with previously reported experiments.

MODEL AND METHODS

In our model, the supramolecular network is formed by n four-armed star-shaped molecules in a well-stirred solution of constant volume $\tilde{V}$. The position of each polymer is tracked by the

coordinates of its junction point $\tilde{r}_i$, $i = 1 \ldots n$. Each arm is a Gaussian chain of N Kuhn steps of length b and friction coefficient ζ_0, and is decorated with an associative group or sticker at the end that can dynamically form connections with other free stickers, as illustrated in Figure 1. The one-dimensional stochastic differential equation to update the position of molecule i is:

$$d\tilde{r}_i = d\tilde{t}\frac{k}{\zeta}\sum_{j=1}^{N_A}(\tilde{a}_{ij} - \tilde{r}_i)l_{ij} + \sqrt{\frac{2k_BT}{\zeta}}d\widetilde{W}_i \qquad (1)$$

where k_B is Boltzmann's constant, T is the temperature, $\widetilde{W}_i$ is a standard Wiener process (Gaussian with zero mean and variance $d\tilde{t}$) [29], $N_A = 4$, $k = k_BT/Nb^2$ is the strength of the spring constant associated with each arm, $\zeta = N_AN\zeta_0$ is the total friction coefficient of the molecule, assumed to act at the junction point, $\tilde{a}_{ij}$ is the attachment point of sticker j of molecule i, and l_{ij} is a Boolean variable that is 0 when the sticker is free or attached to another sticker of the same molecule (forming an intramolecular association or loop) and 1 when it is attached to a sticker in a different molecule (forming an intermolecular association). As a result, the sum only runs over arms that form intermolecular bonds.

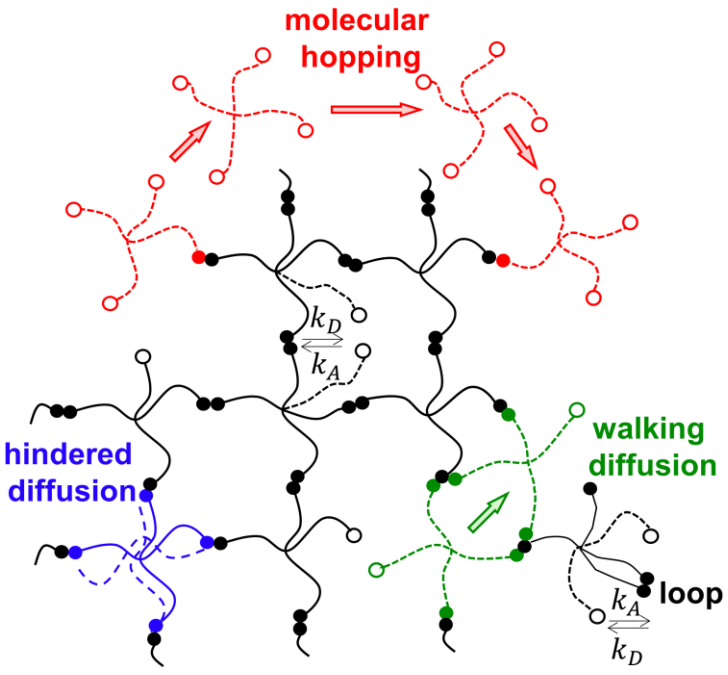

Figure 1: Schematic view of the association reactions (filled/open symbols represent associated/free stickers), the formation of loops and the three main diffusion mechanisms in associating star-shaped polymers.

In previous experiments [10], the polymers are in semidilute conditions and below the entanglement concentration, and star arms can be regarded as Rouse chains of correlation blobs whose size and terminal time scale with concentration according to [30,31]

$$\langle R^2 \rangle = R_g^2 \left(\frac{\phi^*}{\phi}\right)^{\frac{2\nu-1}{3\nu-1}} \quad (2)$$

and

$$\tau_R = \tau_F \left(\frac{\phi^*}{\phi}\right)^{\frac{3\nu-2}{3\nu-1}} \quad (3)$$

where ϕ is the polymer volume fraction (ϕ^* at overlap conditions), R_g^2 and τ_F are the arm size and relaxation time in dilute conditions, respectively, and $\nu = 0.588$ in a good solvent. In the experiments [10], the anomalous diffusive scaling is observed at length and time scales that are much greater than the size (R_g) and Rouse time (τ_R) of the arms, respectively. Therefore, in the model, the internal molecular degrees of freedom are coarse-grained and the arms are treated as Hookean dumbbells. The model represents the center of mass dynamics well even at shorter length and time scales, provided that star arms completely relax their conformation during the time that the associative group is detached (i.e., $1/k_A \gg \tau_R$).

The system is considered to be well stirred so all free stickers can react with each other. It is assumed that the attachment reactions are governed by second order kinetics, whereas the detachment is first order. Note that in the two-state model of Tang el al. [12] and in the three-state model of Rapp et al. [28], association reactions are considered to be first order and pseudo-first order,

respectively. In our model, every time 2 stickers form an intermolecular association, they are linked virtually but each sticker is effectively attached to the background at point $\tilde{\alpha}_{ij}$, which is selected randomly from a Gaussian distribution centered at the junction point of each molecule $\tilde{r}_i$, with variance Nb^2. In this work, fluctuations of the attachment points of stickers have not been considered and, as the concentration is higher than the overlap, depletion effects in the number of intermolecular binding events have been neglected. Whenever two stickers of the same molecule create a loop, they are also linked virtually but not attached to the background, so they do not exert any force to the molecule junction point. The kinetic constants of attachment and detachment are $\tilde{k}_A$ (units of volume/time) and $\tilde{k}_D$ (units of 1/time), respectively. The equilibrium constant of the association is $\tilde{K}_{eq} = \tilde{k}_A/\tilde{k}_D$ (units of volume).

We evolve the associative state of the stickers by means of a stochastic chemical kinetics algorithm.[32] The propensity for intermolecular bonding can be written as:

$$\tilde{\alpha}^B = \frac{\tilde{k}_A}{\tilde{V}} \sum_{i=1}^{n} f_i(F - f_i) \qquad (4)$$

where f_i is the total number of free arms of molecule i, and F is the total number of free arms in the system. The propensity for looping reactions can be written as:

$$\tilde{\alpha}^L = \frac{\tilde{k}_A}{\tilde{V}_{span}} \sum_{i=1}^{n} f_i(f_i - 1) \qquad (5)$$

where $\tilde{V}_{span} = 4\pi\langle R^2\rangle^{\frac{3}{2}}/3 = 4\pi N^{3/2}b^3/3$ is the volume spanned by one molecule and the sum runs over molecules with more than one free arm. At overlap conditions, $\tilde{V} = n\tilde{V}_{span}$, which allows to express the system concentration as $\phi^*/\phi = V/nV_{span} = \tilde{V}/n\tilde{V}_{span}$. The bond dissociation reaction is the same independently of the bond being a loop or an intramolecular association. At

any time, the total number of bonds in the system is equal to $(nN_A - F)/2$, so the total propensity for detachment is:

$$\tilde{\alpha}^D = \frac{\tilde{k}_D}{2}(nN_A - F) \quad (6)$$

Each time step, $\Delta\tilde{t}$, the stochastic differential equation (1) is updated using an explicit Euler-Maruyama first order algorithm [29], and the states of the stickers are updated using the tau-leap algorithm [32,33]. In this algorithm, the number of bonding, looping and detachment reactions are calculated by drawing random numbers from a Poisson distribution with mean and variance given by the product of the corresponding propensities, equations (4), (5) and (6), and the time step $\Delta\tilde{t}$.[30,32] Within each reaction channel (B, L and D), the propensities of all possible reactions are equal, and thus the actual stickers that attach or detach are chosen randomly among all available candidates for each reaction. The simulations are run at equilibrium and the number of molecules n is large enough so that the leap condition is satisfied for the typical time steps used to update molecule positions [33].

The arm size $\sqrt{Nb^2}$ and Rouse time $\tau_R = N\zeta_0/k = N^2\zeta_0 b^2/k_B T$ are chosen as the units of length and time in the system, respectively. In these units, the stochastic differential equation (1) becomes:

$$dr_i = \frac{dt}{\mathrm{N_A}}\sum_{j=1}^{N_A}(a_{ij} - r_i)l_{ij} + \sqrt{\frac{2}{\mathrm{N_A}}}dW_i \quad (7)$$

and the kinetic constants have the following expressions:

$$k_A = \frac{\tau_R}{(Nb^2)^{\frac{3}{2}}}\tilde{k}_A$$
$$k_D = \tau_R\tilde{k}_D \quad (8)$$

$$K_{eq} = \frac{\widetilde{K}_{eq}}{(Nb^2)^{\frac{3}{2}}}$$

The dimensionless volume spanned by a molecule is equal to $V_{span} = 4\pi/3$. The expressions for the non-dimensional propensities are equivalent to equations (4), (5) and (6) but without the tildes. In total, the model has five parameters: k_A, K_{eq}, R_g, τ_F and ϕ.

At every time step Δt, each sticker on the diffusing polymer may undergo one of four possible events (see Figure 1): (1) remain unreacted, (2) form a loop (intramolecular attachment), (3) form a bridge (intermolecular attachment), or (4) detach from a loop or bridge. Sticker association is considered in a mean-field sense: the probability of association of a sticker takes into account the state of all stickers in the system. For each time step, B, L and D reactions and the molecules that react within each channel are sorted randomly to avoid bias.

In FRS measurements [12], two coherent laser beams of wavelength λ cross at an angle θ inside a sample where a small fraction of tracer molecules have been labelled with chromophores. By constructive interference, the laser beams create a one-dimensional sine-shaped interference pattern of period $d = \lambda/2\sin(\theta/2)$ in the sample. The chromophores are bleached in the higher intensity regions of the interference grating, effectively creating a sinusoidal concentration profile of non-bleached molecules. The diffusion of the tracers with time destroys the grating and, by tracking the decay of the scattered intensity of the sample as a function of time, it is possible to extract the characteristic relaxation time $\langle\tau\rangle$ of the system as a function of the grating period d. For a substance diffusing in the Fickian regime, the relationship between $\langle\tau\rangle$ and d^2 is linear with slope given by $1/4\pi^2 D$, where D is the molecular self-diffusion coefficient.

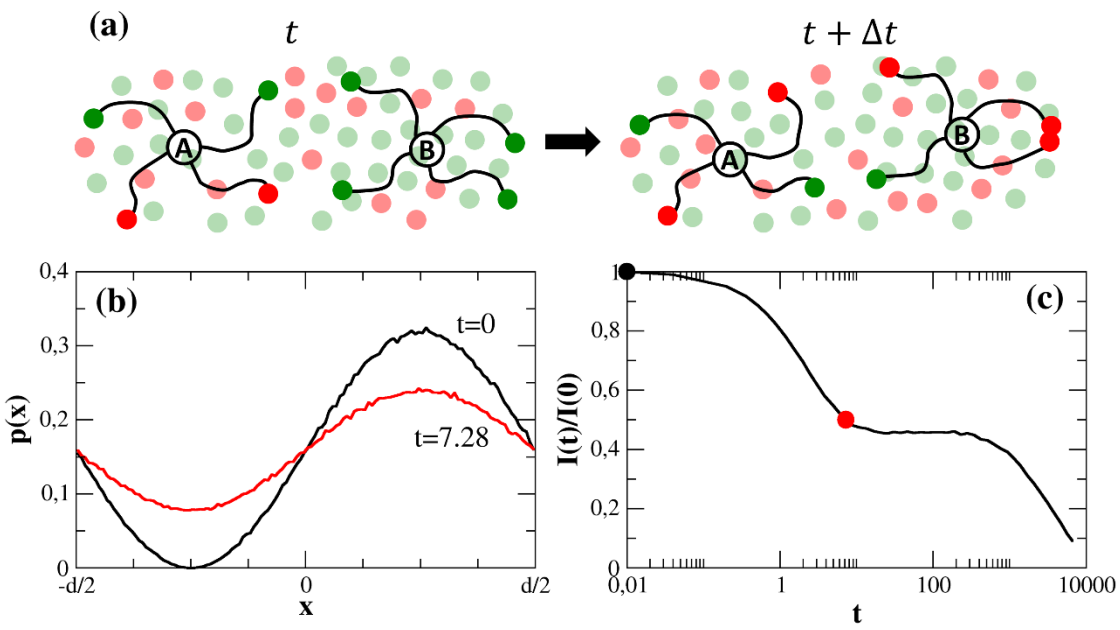

Figure 2: Schematic of the algorithm for the simulation of an FRS experiment. b) Molecules are initially distributed in the domain $[-d/2\,, d/2]$ according to a sinusoidal probability distribution (panel b). a) At time t, molecule A has two free stickers (green dots) and another two attached to the background (red dots), while molecule B has four free stickers. A and B diffuse over a mean-field background made of free and attached stickers (faded green and red dots, respectively), representing the current state all the stickers in the system. During the time step Δt, the centers of mass of A and B move according to Eq. (7) and the states of their stickers, as well as the states of the background stickers, change according to the stochastic reaction rules, with propensities given by Equations (4-6). b) Due to the molecular motion, the density distribution of molecular centers of mass evolves, as seen here for a system of $N = 10^5$ star molecules with 4 arms, $k_A = 0.0025$, $K_{eq} = 5$, at overlap concentration, at times $t = 0$ and $t = 7.28$. c) Normalized intensity decay calculated by Fourier transforming the distributions in (b), with the highlighted times $t = 0$ (black symbol) and $t = 7.28$ (red symbol).

In order to model FRS experiments [10,11,12], a large ensemble $n = 10^5$ of molecules, whose stickers' states have been previously equilibrated, are randomly distributed in a one-dimensional periodic domain of length d with normalized probability distribution $p(x) = (\sin(2\pi x/d) + 1)/d$ that represents the initial one-dimensional sinusoidal concentration profile of bleached dye-label molecules created during the writing interval of the FRS experiment, where d denotes the period of the grating [10,11,12] (see Figure 2b). In order to distribute the molecules randomly according to $p(x)$, we first calculate $P(x) = \int p(x)dx$ and use the standard transformation method described in section 7.2 of Numerical Recipes [34]. Then, the molecules are allowed to evolve (see Figure 2a) and, periodically, a normalized histogram of molecular positions in the 1D domain is built (see Figure 2b). This histogram is Fourier transformed, and the amplitude of the longest mode at that time, $I(t)$, is calculated, which corresponds to the scattered intensity measured in the experiments. The simulations are run at equilibrium; therefore, the distributions of the states of the stickers is constant with time. As molecules diffuse over time, this intensity decays monotonically towards zero (see Figure 2c). To obtain the characteristic time, $\langle\tau\rangle$, an exponential function is fit to the resulting transient $I(t)/I(0)$ data. For intermediate values of d, the intensity shows two relaxation modes. A sum of two exponentials is used to fit $I(t)/I(0)$ and $\langle\tau\rangle$ is determined as the longest of the two relaxation times (details about the fitting procedure are provided in Section 3 of Supporting Information). Resulting characteristic times are then acquired as a function of domain size. It is important to note that, although the distribution of molecules according to $p(x)$ suggests a non-homogeneous density of molecules in the system, the whole ensemble of n molecules represents the equilibrium state of the system at any point in space. The gradient is only in the labeled tracer component. The probabilities of sticker binding are not dependent on the local density of free stickers. Any pair of molecules in the system may become virtually bonded by intermolecular

association, independently of their relative positions in real space. This method to simulate the FRS experiment is fully equivalent to calculating the one-dimensional dynamic structure factor of the position of the junction points as the molecules diffuse in space.

RESULTS AND DISCUSSION

Figure 3a displays a typical plot of the characteristic time, $\langle\tau\rangle$, as a function of domain length squared, $d^2/4\pi^2$, from simulations of four-arm star polymers with $K_{eq} = 5$, $k_A = 0.0025$ and $\phi^*/\phi = 1$. The simulation results demonstrate that this relatively simple molecular model is able to capture both the apparent superdiffusive and large d^2 Fickian regimes observed in experimental measurements [10,11,12].

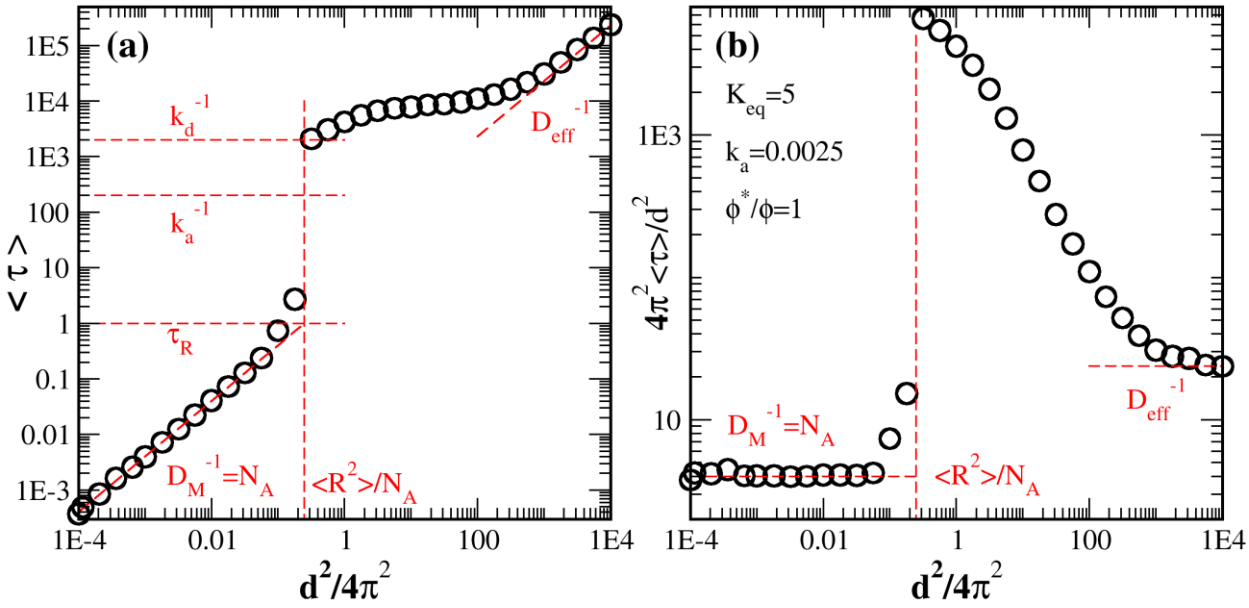

Figure 3: (a) characteristic time $\langle\tau\rangle$ as a function of the domain length from BD simulations of FRS experiments of molecules with 4 arms, $k_A = 0.0025$, $K_{eq} = 5$, at the overlap concentration; and (b) normalized $\langle\tau\rangle$ as a function of the domain length, revealing differences in the early- and large-distance diffusion coefficients, as well as the apparent superdiffusive scaling.

The simulated FRS result contains four regimes: an early Fickian regime, a caging regime, an apparent superdiffusive regime, and a late Fickian regime. Given that $K_{eq} > 1$, at equilibrium most of the stickers are attached to the background. At times much smaller than τ_R (1 in non-dimensional units), the molecules still do not feel the attachment potential and can move freely with diffusion coefficient $D = N_A^{-1}$, up to a maximum distance $\langle R^2 \rangle / N_A$ (N_A^{-1} in non-dimensional units), which corresponds to the maximum mean-square displacement of the center of mass of a molecule that has N_A stickers attached to the background. In this regime, $\langle \tau \rangle$ increases linearly to τ_R with slope equal to $D^{-1} = N_A$. At τ_R, a sharp increase in $\langle \tau \rangle$ is observed due to a caging effect. Attached molecules are trapped in a cage of size $\langle R^2 \rangle / N_A$ and must wait for the arms to detach in order to diffuse over longer distances. For timescales, $\langle \tau \rangle$, larger than the inverse of the detachment rate, k_D^{-1}, stickers can detach from and reattach to the background, moving the molecular center of mass in the process. Motion of the center of mass over distances greater than $\langle R^2 \rangle / N_A$ through sequential detachment and reattachment of individual arms is termed walking. Walking is the most frequently observed diffusion event due to the relatively high likelihood of single arm detachment events. Infrequently, some molecules may also detach all their stickers and diffuse freely throughout the network in a process referred to as hopping. During this rare event, molecules diffuse with diffusion constant $D = N_A^{-1}$. It is hypothesized that, in order to observe superdiffusive scaling in FRS experiments, hopping must be faster than the walking mechanism over large distances. For that to occur, the distance travelled by molecules during hopping events must be much larger than the molecular radius of gyration, which is the characteristic size of a walking step. In the crossover between the early and late Fickian regimes, the interplay between walking and hopping modes dictates the prominence and shape (i.e., amplitude and inflection) of the apparent superdiffusive regime. At large d^2, the polymers again exhibit Fickian diffusion, but

now with an effective diffusivity, D_{eff}, that contains contributions from the walking and hopping mechanisms.

Differences in diffusivity between the two limiting Fickian regimes and the non-Fickian behavior at intermediate length scales are highlighted in Figure 3b, where the primary ordinate, $\langle\tau\rangle$, is renormalized by the abscissa, $d^2/4\pi$. Diffusion coefficients in the short and long length scale Fickian regimes are now given by the inverse of the plateau values. *A priori* calculation of self-diffusion coefficients in both Fickian regimes is provided in Section 2 of Supporting Information.

The results from the simulations agree qualitatively with the experimental data at large d^2 values [12] (current experiments cannot resolve the early time Fickian diffusion and caging regimes). In the simulations, the escape from the cage occurs at $d^2 \approx 4\pi^2\langle R^2\rangle$, which is 1-2 orders of magnitude larger than the molecular size. The exact location of the large d^2 Fickian regime depends on the values of k_A and K_{eq}. In the particular example shown in Figure 3, this regime is observed at d^2 values that are 4-5 orders of magnitude larger than the molecular size, in reasonable qualitative agreement with the experiments.

A comparison of FRS simulations and mean-square displacement measurements shows that this unexpected regime is not observed in the mean-square displacement. In Figure 4a, the mean-square displacement of the center of mass of molecules with 4 arms, $k_A = 0.0025$, $K_{eq} = 5$, and at the overlap concentration (same case as Figure 3) is shown. Early and late Fickian diffusion regimes are clearly observed, with self-diffusion coefficients that agree well with those extracted from Figure 3. However, no superdiffusive scaling is observed in the crossover regime. Instead, a clear subdiffusive regime is found, as shown in Figure 4b, where the mean-square displacement is divided by time. Comparison between Figures 2 and 3 shows that the caging regime observed in

the FRS simulation corresponds in timescale to the subdiffusive regime observed in the mean-square displacement; both the apparent superdiffusive and late Fickian regimes in the FRS simulation occur within the late Fickian regime of the mean-square displacement plot. Therefore, FRS results are more sensitive to the molecular association mechanisms than mean-square displacement, and the $\langle\tau\rangle$ vs d^2 plot shows richer features than the $\langle r^2\rangle$ vs t plot, even though both methods are sampling different moments of the same distribution of displacements of the same physical model.

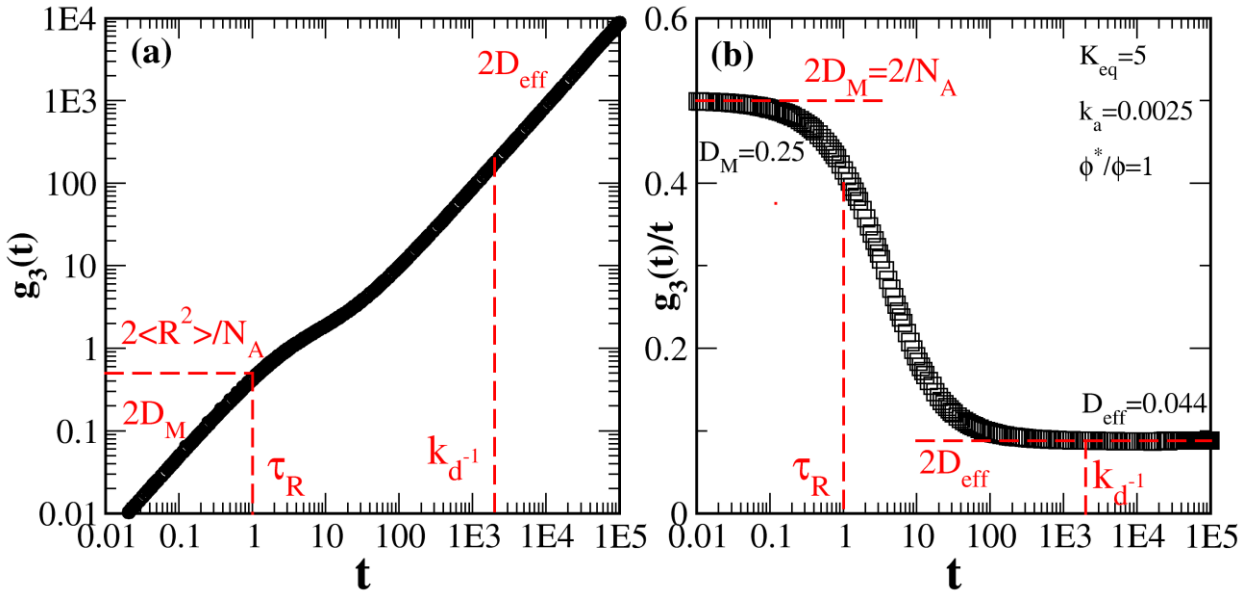

Figure 4: (a) Mean-square displacement of the center of mass, $g_3(t)$, as a function of time from BD simulations of molecules with 4 arms, $k_A = 0.0025$, $K_{eq} = 5$, at the overlap concentration. (b) $g_3(t)$ divided by time, highlighting the early and late Fickian behavior, as well as the subdiffusive regime in the crossover.

To illustrate the origin of these differences, the probability distribution of the center of mass displacement as a function of time for molecules with 4 arms, $k_A = 0.0025$, $K_{eq} = 5$, and at the overlap concentration (same case as Figures 3 and 4) is shown in Figure 5a. When $t \leq \tau_R$, the molecules are trapped in the cage and the distribution is Gaussian, as proved by the small values

of the one-dimensional non-Gaussian parameter [35] $\alpha = \langle r^4 \rangle / 3\langle r^2 \rangle^2 - 1$ shown in Figure 5b. At times $t \geq 10\tau_R$, the distribution becomes bimodal, with a Gaussian mode of small variance that represents the molecules that have not been able to detach completely from the background and therefore have very small diffusivity, and a second mode that represents the displacement of molecules that have escaped the cage by means of the walking and hopping mechanisms. In this time region, the parameter $\alpha > 1$ indicating a non-Gaussian distribution, and superdiffusive scaling is observed in the FRS experiments. At times $t \gg k_D^{-1}$, the parameter α decreases slowly to zero and the second Fickian regime is observed. The FRS simulations show an apparent superdiffusive regime while the mean-square displacement does not because the FRS simulations sample a different moment of the distribution of molecular motion (the one-dimensional dynamic structure factor of an isotropic system is equivalent to the average $\langle \cos(qr) \rangle$) that is more sensitive to the distribution of diffusivities while the mean-square displacement ($\langle r^2 \rangle$) is sensitive just to the average. Both ways of looking at the same molecular motion are qualitatively very similar up to the point when the molecules escape from the caging regime (in fact, up to that regime, one plot is approximately the reflection of the other by the diagonal line $y = x$). At longer times, the mean-square displacement of the system can be much larger than the size of the cage if a small fraction of molecules detaches from the network and diffuses over very long distances. However, in FRS measurements, when the period of the grating is larger than the molecular size, a large fraction of molecules must diffuse over distances of the order of d^2 in order to destroy the sinusoidal distribution of unbleached chromophores. For that to happen, the system needs to wait a very long time. Therefore, FRS is more sensitive to the large displacement tail of the distribution, providing a very important probe into molecular dynamics that complements other methods of measuring diffusion.

In understanding this effect, it is very illustrative to compare to the family of models originally proposed by Tang, Wang, and Olsen and Tirrell and coworkers. These models are continuum models of reaction-diffusion which are represented by one differential equation for each diffusing species, and the species are allowed to interconvert according to the laws of chemical kinetics. When mean-square displacement is plotted for any member of this family, only Fickian behavior is observed, where the diffusivity is an average of all the different species based on their relative abundance. While the average remains unchanged from a single effective species, the distribution of displacements changes substantially, showing a peak for the abundant, slow species and a long tail for the rare, fast diffusive events. The FRS measurement is therefore extremely useful in understanding different molecular mechanisms because it can differentiate between the single effective species and the multiple different species.

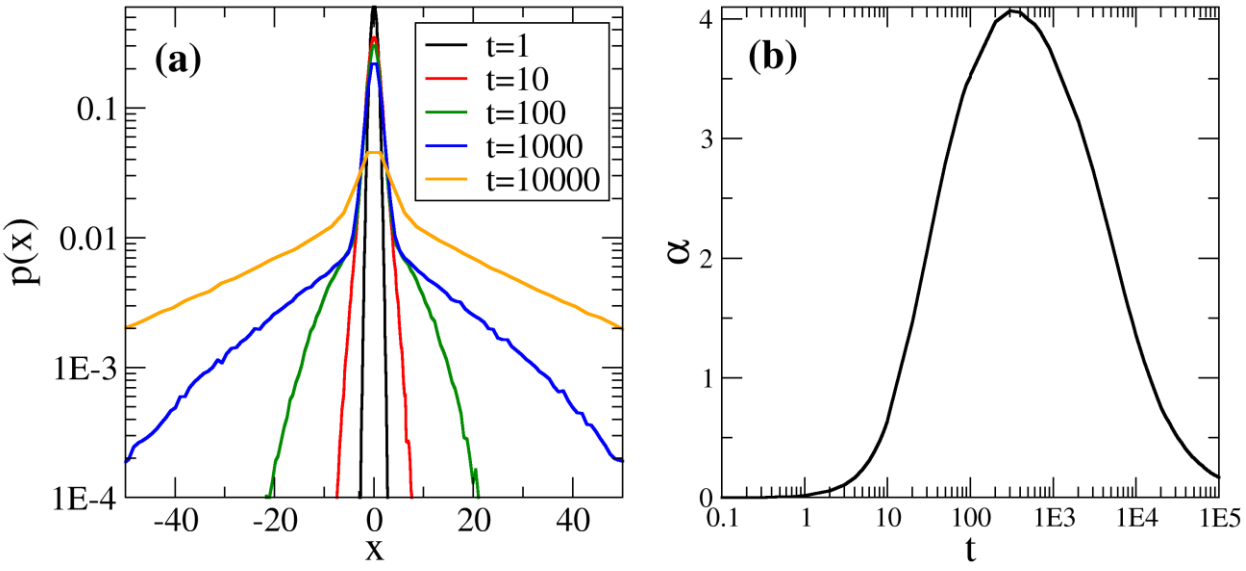

Figure 5: (a) Probability distribution of the motion of the center of mass of molecules with 4 arms, $k_A = 0.0025$, $K_{eq} = 5$, at the overlap concentration. (b) Time evolution of the one-dimensional non-Gaussian parameter $\alpha = \langle r^4 \rangle / 3\langle r^2 \rangle^2 - 1$ for the same system.

Comparing diffusion rates via different molecular mechanisms enables scaling relationships to be derived that estimate the range of molecular parameters over which the apparent superdiffusive regime can be observed. At large length and time scales, the effective diffusion coefficient D_{eff} has contributions from both walking and hopping mechanisms (Figure 1). Hopping diffusion can be calculated as the product of the diffusion constant of a free molecule, $D = 1/N_A$, times the probability that a molecule is completely detached from the network. Walking diffusion can be estimated by means of a simple scaling argument. During a walking event, a molecule that has j stickers bonded to the background detaches one with attempt frequency k_D. The mean-squared displacement of the center of mass during the walking step, before the free arm gets bonded again, is given by the size of the arms $\langle R^2 \rangle$ divided by the number of arms that remain attached to the network, i.e. $\langle R^2 \rangle / (j-1)$ (equal to $1/(j-1)$ in the units of the simulation). Therefore, the diffusion coefficient of a molecule walking on j arms is $k_D/(j-1)$. A molecule can walk on $j = 2 \ldots N_A$ arms (when it has just one arm attached to the background, detachment leads to a hopping event), and each of the walking contributions must be multiplied by the probability of having j arms attached to the background. The scaling argument above assumes that walking occurs by detaching and re-attaching a single arm at a time (i.e. it neglects rare but important events such as when a molecule goes from $j \to j-1 \to j-2$ arms attached). For $K_{eq} \gg 1$, it is more likely that a molecule will attach a free arm back to the background before it detaches a second one. The resulting effective diffusion coefficient of the walking and hopping mechanisms is:

$$D_{eff} = D_{walk} + D_{hop} = \sum_{j=2}^{N_A} p_j k_D \frac{\langle R^2 \rangle}{j-1} + \frac{p_0}{N_A} \qquad (9)$$

where p_j is the probability that a molecule has j arms attached to the background. Although Eq. (9) is approximate, it successfully permits quantitative prediction of diffusivities in the large

length-scale regime as a function of a wide variety of parameters including K_{eq}, k_A, N_A and concentration (see Section 2 of the Supporting Information).

A general criterion for observing the apparent superdiffusion emerges by examining the curve shape as it exits the caging regime. In the case of no superdiffusive scaling, molecules should exhibit Fickian scaling immediately following the caging regime, at the point $d^2/4\pi^2 = 1/N_A$ and $\langle\tau\rangle = k_D^{-1}$. The self-diffusion coefficient of such Fickian process would be equal to k_D/N_A (see dashed blue line in Figure 6a). For the apparent superdiffusive scaling to be observed, the effective diffusion coefficient at large distances should exceed that of the limiting Fickian-scaling described above, or

$$D_{eff} \gg \frac{k_D}{N_A} = \frac{k_A}{N_A K_{eq}} \qquad (10)$$

which corresponds to the hypothetical diffusion coefficient of a molecule walking on $N_A + 1$ arms.

Although both walking and molecular hopping contribute to D_{eff}, the apparent superdiffusive scaling is most easily observed when molecular hopping is the primary diffusive mode, as illustrated in Figure 6a. When hopping is switched off in the simulations, the apparent superdiffusive scaling is still observed but to a lesser extent. The ability to form loops enhances diffusion, as seen in Figure 6a, by effectively reducing the number of arms that need to be detached in order to hop, and by increasing the walking diffusivity. When molecular hopping is prevalent, $D_{hop} \gg D_{walk}$ and $D_{eff} \approx D_{hop} = p_0/N_A$. In this case, the criterion for observing superdiffusive scaling in Eq. (10) becomes $k_A \ll p_0 K_{eq}$, where p_0 depends on the number of arms and the equilibrium constant of the attachment reactions. The calculation of the probabilities p_j can be difficult, in the full model, but they can be easily estimated if the looping reactions are turned off

(see Section 4 of Supporting Information). In that case, $p_0 \approx K_{eq}^{-N_A/2}$, so the requirement for observing superdiffusive scaling in the absence of looping becomes

$$k_A \ll K_{eq}^{1-N_A/2} \qquad (11)$$

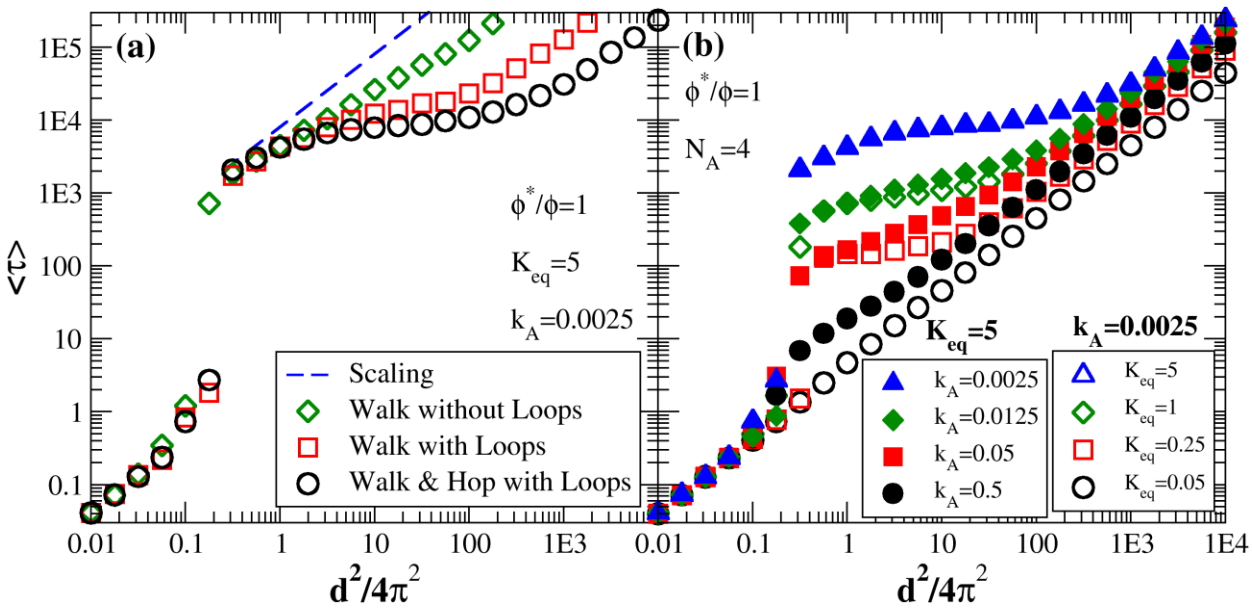

Figure 6: (a) $\langle\tau\rangle$ versus $d^2/4\pi^2$ for $N_A = 4$, $\phi^*/\phi = 1$, $K_{eq} = 5$ and $k_A = 0.0025$, with all diffusion mechanisms (black symbols), only walking mechanisms (red symbols), only walking mechanisms with loops forbidden (green symbols) and limiting inverse effective diffusion coefficient N_A/k_D when no superdiffusive scaling is observed (blue dashed line). (b) $\langle\tau\rangle$ versus $d^2/4\pi^2$ $N_A = 4$, $\phi^*/\phi = 1$, varying k_A at fixed $K_{eq} = 5$ (closed symbols), and varying K_{eq} at fixed $k_A = 0.0025$ (open symbols).

Although approximate, Eq. (11) reveals that superdiffusive scaling is less prevalent for star polymers containing many arms and for large values of the association equilibrium constant. Figure 6b, which plots the average characteristic time, $\langle\tau\rangle$, versus d^2 for four-arm star polymers at fixed concentration as a function of k_A (with constant K_{eq}) and K_{eq} (with constant k_A),

respectively, clearly shows that the simulation results are consistent with this scaling prediction. The values of k_A and K_{eq} in both plots have been chosen to give identical inverse detachment times, k_D. In Figure 6b, superdiffusive scaling is observed when $k_A < 0.1$ in good agreement with Eq. (11), despite the presence of looping. For $k_A > 0.1$, superdiffusive scaling is less easily observed as indicated by Eq. (11). Walking diffusion becomes the prevalent diffusive mode, since D_{walk} increases strongly with increasing k_A, while D_{hop} is independent of k_A in Eq. (9). Superdiffusive scaling is observed for values of $K_{eq} > 1$ as expected because an associated network is required to produce differing diffusive mechanisms. The range of length scales over which the superdiffusive scaling is observed widens for increasing values of K_{eq}.

Loop formation increases the probability of hopping, increasing the likelihood of star polymers exhibiting superdiffusive scaling. The balance between intermolecular and intramolecular association of stickers is primarily governed by concentration. This effect is highlighted in Figure 7a, where $\langle\tau\rangle$ versus d^2 is shown for constant values of k_A and K_{eq}, at different polymer volume fractions. Below the overlap concentration ($\phi^*/\phi > 1$), looping is highly probable and hopping is more likely. As concentration increases above the overlap concentration ($\phi^*/\phi < 1$), hopping becomes increasingly difficult because star arms of different molecules interpenetrate and intermolecular associations are more likely. In Figure 7a, the width of the apparent superdiffusive region becomes narrower as the concentration of polymers increases, until it disappears completely for ($\phi^*/\phi < 0.1$). The diffusion behavior of a concentrated solution ($0.1 < \phi^*/\phi < 0.25$) is qualitatively similar to that of a solution at the overlap concentration for which looping reactions have been turned off.

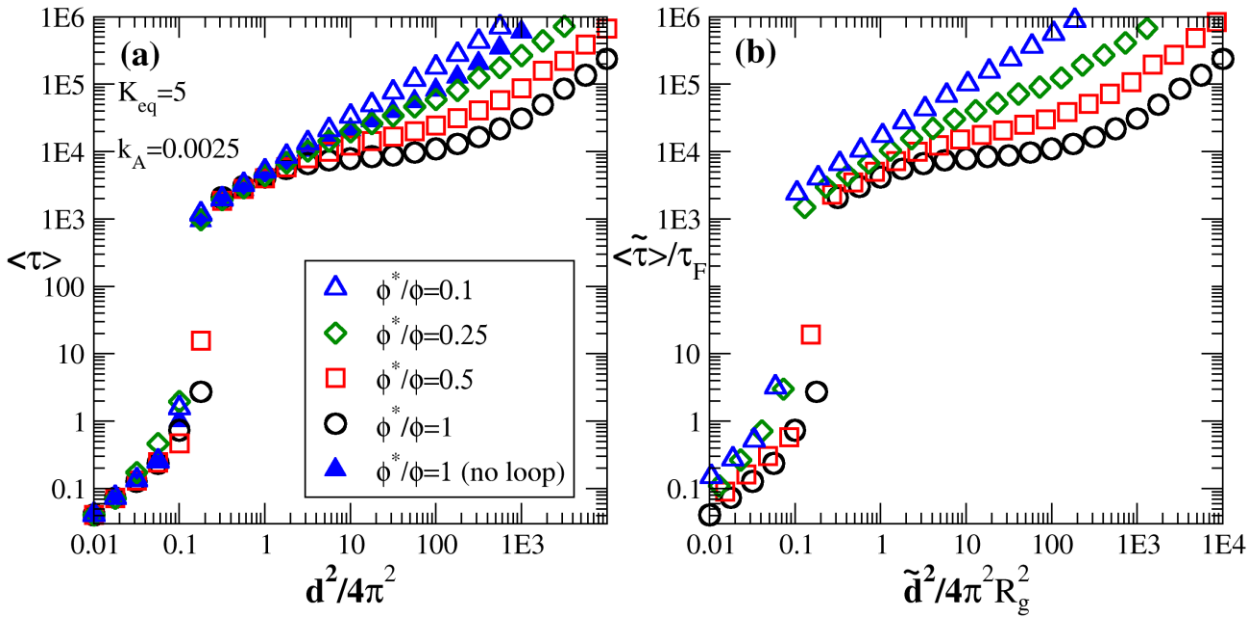

Figure 7: (a) $\langle\tau\rangle$ versus $d^2/4\pi^2$ for varying concentration, expressed as the ratio of the overlap volume fraction to the system volume fraction, ϕ^*/ϕ, with fixed $k_A = 0.0025$, $K_{eq} = 5$, for molecules with $N_A = 4$ arms and loops allowed (open symbols). Filled symbols show a case in which loop reactions are not allowed. (b) Same results represented for real units, taking into account the scaling of the molecular size and relaxation time given by Equations (2) and (3).

In semidilute conditions, according to Equations (2) and (3), changes in concentration affect the molecular size and relaxation time, used as basic units of length and time in our simulations. In a good solvent, the arm size decreases with concentration, whereas the relaxation time increases. In Figure 7b, the non-dimensional simulation results of Figure 7a are shown in real units, scaled by the size, R_g, and relaxation time, τ_F, of the arms in dilute conditions. Higher concentrations have a smaller cage size and slower diffusion constants. The $\langle\tilde{\tau}\rangle$ vs $\tilde{d}^2$ curves are more spread out than the same curves in non-dimensional units.

In order to test the validity of the assumptions of the model, the theoretical predictions have been compared to experimental FRS measurements of four-arm poly(ethylene glycol) star polymers of

M_w = 10,000 g/mol, end-functionalized with terpyridine which associating with divalent Zn^{2+} ions in N,N-dimethylformamide, a good solvent for the polymer. [10] The units of length and time in the simulations are rescaled using Eqs. (8) and (9), respectively, and the values of the non-dimensional rate and equilibrium constants are modified accordingly. Overall, the model has five fitting parameters: K_{eq}, k_A, R_g, τ_F and ϕ. To reduce the complexity of the fitting procedure, the concentration ϕ is fixed based upon the experimental conditions, and the other four parameters are fit to the data. Figure 8a compares experimental data of Tang et. al [10] with the simulation results for the best-fit parameter set, values of which are included in the inset to the figure. Here, each theoretical point corresponds to a separate FRS simulation. In all cases, simulation results are in good qualitative agreement with experimental data over several decades of length and time, and at several polymer concentrations, using only the single set of fitting parameters.

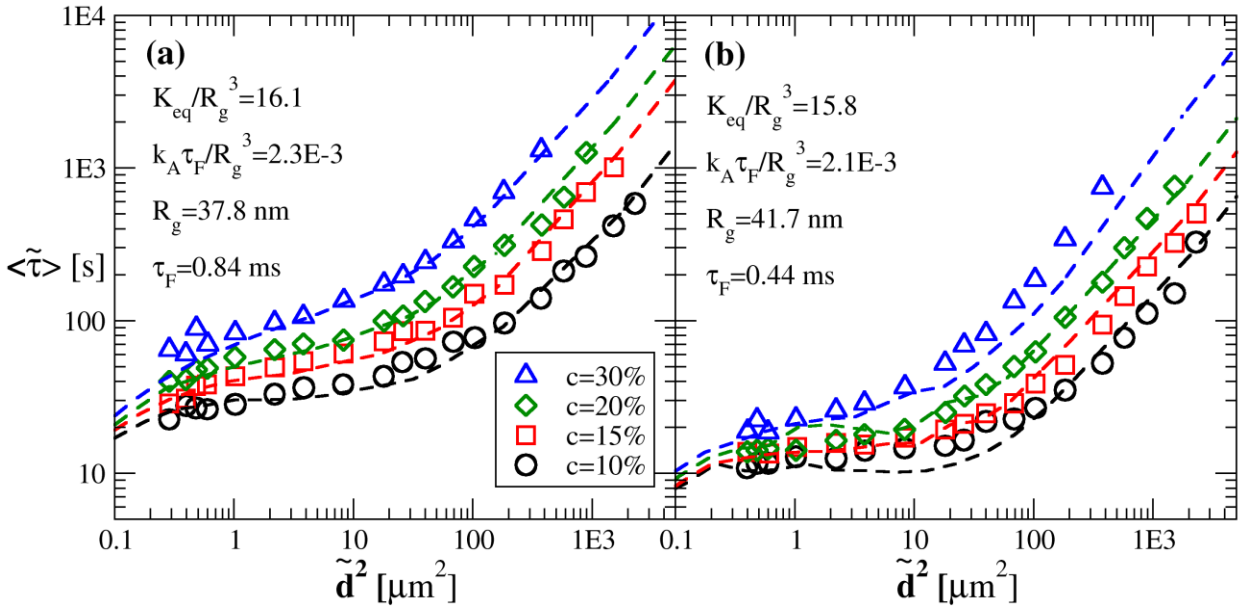

Figure 8: (a) Simultaneous fit of the theory to experimental self-diffusion data of telechelic 4-arm PEG stars at different concentrations, see Tang el al. [10]. (b) Fit to experimental data of tracer diffusion of 3-arm star tracers through a 4-arm star gel matrix, see Tang el al. [10].

In Figure 8b, the simulation results are fit to experimental measurements of four-arm tracer molecules with only three stickers diffusing in a mesh of four-arm molecules with four stickers. The predictions of the model have been calculated by diluting 2% of molecules with 4 arms and only three stickers in a matrix of stars with 4 stickers, following the same approach as in the experiment. The agreement of the theory with the experimental data is also good, and manages to capture the faster diffusion and the sharper transition from the superdiffusive scaling to the Fickian regime at long distances. The fitting is somewhat noisier in this case because fewer molecules are used and the statistics are poorer. The values of the fitting parameters are very similar in both cases.

In contrast to the phenomenological two-state theory proposed previously [12], the parameters of extracted by fitting the simulations have a well-defined molecular interpretation given by the development of the model. In Figure 8a, however, the obtained values of $\tau_F = 0.84$ ms and $R_g = 37.8$ nm are unexpectedly large for the molecular weight of the star arms in the experiments (in [19] the value of R_g is estimated as 3.5 nm). Given the approximations inherent in the highly coarse-grained view of the polymers and bond kinetics and the many approximations necessary to map the parameters of the experiment to the simulation, this is reasonable qualitative agreement with the experimental result. However, it is clear that further advances can improve the accuracy of the predictions. Including junction fluctuations may also increase the effective size of the cage and reduce the value of the parameter R_g needed to fit the data, bringing it closer to the experimentally determined values. However, this effect alone cannot account for the one order of magnitude difference between the experimental and the fitted values of R_g. Alternately, even though the model is formulated with a single molecule in mind, it is possible that in the experiments the same

molecular mechanisms described above occur for bundles of a few molecules, with corresponding larger size and relaxation time.

CONCLUSIONS

Four-arm star polymers were modeled as point particles that associate with a mean field polymer network through massless associative arms, enabling simulation of self-diffusion of these molecules at length scales larger than the polymer size. The simulation results reveal the importance of multiple mechanisms of molecular motion to traverse distances larger than the molecular scale, particularly walking and hopping. The molecular model establishes that previously reported superdiffusive scaling regimes result primarily from molecular hopping which occurs when the kinetics of attachment are slower than the relaxation time of dangling strands. The role of these different molecular mechanisms is particularly clear in FRS data because of its sensitivity to the tail of the displacement distribution caused by rare but long-distance hopping events. The presence of looping defects within the networks strongly promotes hopping by allowing a molecule to effectively reduce the total number of elastically effective connections with the network. Because different measures of diffusion such as mean square displacement and FRS measurement are sensitive to different moments of the displacement distribution, the diffusive process may simultaneously show characteristics of both superdiffusive and subdiffusive behavior depending upon how it is measured.

These findings can be generalized to more complex associating networks with polydisperse arm length, other chain topology, chain statistics, and association kinetics. Separately quantifying the mechanisms of molecular diffusion in this work enables decoupling their impacts, which is essential to developing correlations between molecular and macroscopic transport properties,

predicting material properties *de novo*, and aiding in the development of novel polymeric materials for next-generation applications.

ASSOCIATED CONTENT

Supporting Information. An electronic supplementary information document is available. It contains the following supporting data: a) effect of ensemble size in the simulation results; b) validation of the model and method in simple cases; c) detailed analysis of the intensity decay in simulations of FRS experiments; d) review of scaling arguments in semidilute polymer solutions; e) details of the calculation of volume fractions in experimental data and f) detailes about the methodology to fit the data.

AUTHOR INFORMATION

Corresponding Author

Professor Bradley Olsen, Ph.D., Department of Chemical Engineering, Massachusetts Institute of Technology, 77 Massachusetts Avenue, Room 66-558A Cambridge, MA, 02139, USA.

Tel: +1 617-715-4548

E-mail address: bdolsen@mit.edu

Author Contributions

The manuscript was written through contributions of all authors. All authors have given approval to the final version of the manuscript. All authors contributed equally.

Funding Sources

National Science Foundation Award DMR-1709315.

ACKNOWLEDGMENT

This work was supported by the National Science Foundation under award number DMR-1709315. JR acknowledges funding from Real Colegio Complutense at Harvard and from grant FIS2016-78847-P of the MEC. The authors acknowledge the computer resources and technical assistance provided by the Centro de Supercomputacion y Visualizacion de Madrid (CeSViMa).

REFERENCES

(1) Zhang, P.; Huang, W.; Jia, Z.; Zhou, C.; Guo, M.; Wang, Y. Conformation and adsorption behavior of associative polymer for enhanced oil recovery using single molecule force spectroscopy. *Journal of Polymer Research* **2014,** *21,* 523.

(2) Lee, K.Y.; Mooney, D.J. Hydrogels for Tissue Engineering. *Chemical Reviews* **2001,** *101,* nº 7, 1869–1880.

(3) Glassman, M.J.; Chan, J.; Olsen, B.D. Reinforcement of Shear Thinning Protein Hydrogels by Responsive Block Copolymer Self-Assembly. *Advanced Functional Materials* **2013,** *23,* 1182-1193.

(4) Lu, H.D.; Charati, M.B.; Kim, I.L.; Burdick, J.A. Injectable shear-thinning hydrogels engineered with a self-assembling Dock-and-Lock mechanism. *Biomaterials* **2012,** *33,* 2145-2153.

(5) Chen, Q.; Zhu, L.; Chen, H.; Yan, H.; Huang, L.; Yang, J.; Zheng, J. A Novel Design Strategy for Fully Physically Linked Double Network Hydrogels with Tough, Fatigue Resistant, and Self-Healing Properties. *Advanced Functional Materials* **2015,** *25,* nº 10, 1598.

(6) An, S.Y.; Arunbabu, D.; Noh, S.M.; Song, Y.K.; Oh, J.K. Recent strategies to develop self-healable crosslinked polymeric networks. *Chemical Communications* **2015,** *51,* 13058-13070.

(7) Seiffert, S.; Sprakel, J. Physical chemistry of supramolecular polymer networks. *Chemical Society Reviews* **2012,** *41,* 909-930.

(8) Appel, E.A.; del Barrio, J.; Loh, X...; Scherman, O.A. Supramolecular polymeric hydrogels. *Chemical Society Reviews* **2012,** *41,* 6195-6214.

(9) Holten-Andersen, N.; Harrington, M.J.; Birkedal, H.; Lee, B.P.; Messersmith, P.B.; Lee, K.Y. C.; Waite, J.H. pH-induced metal-ligand cross-links inspired by mussel yield self-healing polymer networks with near-covalent elastic moduli. *Proceedings of the National Academy of Sciences* **2011,** *108,* 2651-2655.

(10) Tang, S.; Habicht, A.; Li, S.; Seiffert, S.; Olsen, B.D. Self-Diffusion of Associating Star-Shaped Polymers. *Macromolecules* **2016,** *49,* 5599-5608.

(11) Tang, S.; Olsen, B.D. Relaxation Processes in Supramolecular Metallogels Based on Histidine–Nickel Coordination Bonds. *Macromolecules* **2016,** *49,* 9163-9175.

(12) Tang, S.; Wang, M.; Olsen, B.D. Anomalous Self-Diffusion and Sticky Rouse Dynamics in Associative Protein Hydrogels. *Journal of the American Chemical Society* **2015,** *137,* 3946-3957.

(13) Yang, L.; Tan, X.; Wang, Z.; Zhang, X. Supramolecular Polymers: Historical Development, Preparation, Characterization, and Functions. *Chemical Reviews* **2015,** *115,* 7196-7239.

(14) Annable, T.; Buscall, R.; Ettelaie, R.; Whittlestone, D. The rheology of solutions of associating polymers: Comparison of experimental behavior with transient network theory. *Journal of Rheology* **1993,** *37,* 695-726.

(15) Tanaka, F.; Edwards, S.F. Viscoelastic properties of physically crosslinked networks: Part 1. Non-linear stationary viscoelasticity. *Journal of Non-Newtonian Fluid Mechanics* **1992,** *43,* 247-271.

(16) Tanaka, F.; Edwards, S.F. Viscoelastic properties of physically crosslinked networks: Part 2. Dynamic mechanical moduli. *Journal of non-Newtonian fluid mechanics* **1992,** *43,* 273-288.

(17) Tanaka, F.; Edwards, S.F. Viscoelastic properties of physically crosslinked networks: Part 3. Time-dependent phenomena. *Journal of non-Newtonian fluid mechanics* **1992,** *43,* 289-309.

(18) Hackelbusch, S.; Rossow, T.; van Assenbergh, P.; Seiffert, S. Chain Dynamics in Supramolecular Polymer Networks. *Macromolecules* **2013,** *46,* 6273-6286.

(19) Rossow, T.; Habicht, A.; Seiffert, S. Relaxation and dynamics in transient polymer model networks. *Macromolecules* **2014,** *47,* 6473-6482.

(20) Green, M.; Tobolsky, A. A new approach to the theory of relaxing polymeric media. *The Journal of Chemical Physics* **1946,** *14,* 80-92.

(21) Tripathi, A.; Tam, K.C.; McKinley, G.H. Rheology and dynamics of associative polymers in shear and extension: theory and experiments. *Macromolecules* **2006,** *39,* 1981-1999.

(22) Rubinstein, M.; Semenov, A.N. Thermoreversible gelation in solutions of associating polymers. 2. Linear dynamics. *Macromolecules* **1998,** *31,* 1386-1397.

(23) Leibler, L.; Rubinstein, M.; Colby, R.H. Dynamics of reversible networks. *Macromolecules* **1991,** *24,* 4701-4707.

(24) Cates, M. Reptation of living polymers: dynamics of entangled polymers in the presence of reversible chain-scission reactions. *Macromolecules* **1987,** *20,* 2289-2296.

(25) Shen, W.; Zhang, K.; Kornfield, J.A.; Tirrell, D.A. Tuning the erosion rate of artificial protein hydrogels through control of network topology. *Nature Materials* **2006,** *5,* 153-158.

(26) Cordier, P.; Tournilhac, F.; Soulie-Ziakovic, C.; Leibler, L. Self-healing and thermoreversible rubber from supramolecular assembly. *Nature* **2008,** *451,* 977-980.

(27) Chaudhuri, O.; Gu, L.; Klumpers, D.; Darnell, M.; Bencherif, S.A.; Weaver, J.C.; Huebsch, N.; Lee, H.-p. ; Lippens, E.; Duda, G.N. Hydrogels with tunable stress relaxation regulate stem cell fate and activity. *Nature materials* **2016,** *15,* 326-334.

(28) Rapp, P.B.; Omar, A.K.; Shen, J.J.; Buck, M.E.; Wang, Z.-G. ; Tirrell, D.A. Analysis and Control of Chain Mobility in Protein Hydrogels. *Journal of the American Chemical Society* **2017,** *139,* 3796-3804.

(29) Öttinger, H. C. *Stochastic Processes in Polymeric Fluids,* Berlin: Springer-Verlag, 1996.

(30) de Gennes, P.-G. *Scaling concepts in polymer physics,* Ithaca: Cornell university press, 1979.

(31) Rubinstein, M.; Colby, R.H. *Polymer physics,* New York: Oxford University Press, 2003.

(32) Gillespie, D. T. Stochastic Simulation of Chemical Kinetics. *Annual Review of Physical Chemistry* **2007,** *58,* 35-55.

(33) Cao, Y.; Gillespie, D.T.; Petzold, L.R. Efficient step size selection for the tau-leaping simulation method. *The Journal of chemical physics* **2006,** *124,* 044109.

(34) Press, W.H.; Teukolsky, S.A.; Vetterling, W.T.; Flannery, B.P. *Numerical Recipes in C (2Nd Ed.): The Art of Scientific Computing,* New York: Cambridge University Press, 1992.

(35) Kumar, S.K.; Szamel, G.; Douglas, J.F. Nature of the breakdown in the Stokes-Einstein relationship in a hard sphere fluid. *The Journal of Chemical Physics* **2006,** *124,* 214501.

(36) Asmussen, S.; Glynn, P.W. *Stochastic simulation: algorithms and analysis,* New York: Springer, 2007.

(37) van Gunsteren, W.F.; Berendsen, H.J. C. Algorithms for Brownian dynamics. *Molecular Physics* **1982,** *45,* 637-647.

FOR TABLE OF CONTENTS USE ONLY

TOC GRAPHIC

The graphic should be provided in the actual size to be used that will fit in an area 3.25 in. wide by 1.375 in. high (8.3 cm × 3.5 cm).